The *Journal of Cotton Science 25:167–183 (2021)*
http://journal.cotton.org, © The Cotton Foundation 2021

TEXTILE TECHNOLOGY

Fourier Transform Infrared Spectroscopic Analysis in Applied Cotton Fiber and Cottonseed Research: A Review

Zhongqi He* and Yongliang Liu

ABSTRACT

Cotton, one of the most important and widely grown crops in the world, is a well-traded agricultural commodity primarily for textile fiber purposes. In addition, cottonseed (a byproduct of fiber production) has been used as an agro-based raw material for manufacturing bio-friendly and sustainable products. Qualitative and quantitative characterization of cotton biomass products/byproducts is an important research area for quality monitoring, improvement, and enhanced use. Fourier transform infrared (FT-IR) spectroscopy is a nondestructive instrumental technique widely used in applied cotton fiber and cottonseed research. This review synthesizes and analyzes the latest developments using FT-IR spectroscopy in investigation of cotton fiber and three cottonseed components (oil, meal/protein, hull) that are impacted by various genetic, cropping, post-harvest processing, and end-use parameters and conditions. Increased knowledge from this review could provide insight and vision in future FT-IR research for the chemistry and quality-evolving mechanisms of these cotton biomass products and their end-uses.

Cotton is one of the most important agricultural commodities globally, primarily for its naturally produced cellulosic textile fibers (Wakelyn and Chaudrey, 2010). Cotton fiber (or lint) is produced from protodermal cells on the outer integument layer of fertilized cottonseed. Its development is divided into four overlapping but distinctive phases: 1) initiation, 2) primary cell wall (PCW) formation for fiber elongation, 3) secondary cell wall (SCW) biosynthesis for cellulose deposition and cell wall thickening, and 4) maturation. It takes approximately 1.5 to 2 months from phase 1 to phase 4 to produce fully mature or developed fibers depending on environmental conditions (Fang and Percy, 2015; Gordon and Hsieh, 2007). Cellulose is the dominant chemical component in mature fibers, accounting for 88.0 to 96.5% of fiber biomass. Mature fibers contain more cellulose and fewer non-cellulosic components than immature fibers. In commercial cottons, immature fibers are responsible for fiber entanglement during mechanical processing and degrading the desired color appearance in dyed yarn and finished fabric products (Fang and Percy, 2015; Wakelyn et al., 2007).

In addition to cotton fiber, other types of cellulosic biomass byproducts are available from cotton plants before and after seed cotton harvesting (Fig. 1). Recent studies have shown that these biomass byproducts are also useful as a soil amendment, animal feed supplement, bioenergy source, and industrial raw material (He et al., 2014b, 2016, 2018b; Kirkan et al., 2018; Kutlu and Kocar, 2018; Ren et al., 2015). Egbuta et al. (2017) reviewed the phytochemical properties associated with different parts of cotton plants (leaves, bolls, stalks, and stems) and their biological activities to promote the full exploitation of cotton biomass products. In general, cotton biomass mainly arises from different levels of complex polymers, including but not limited to cellulose, hemicellulose, pectins, and lignins.

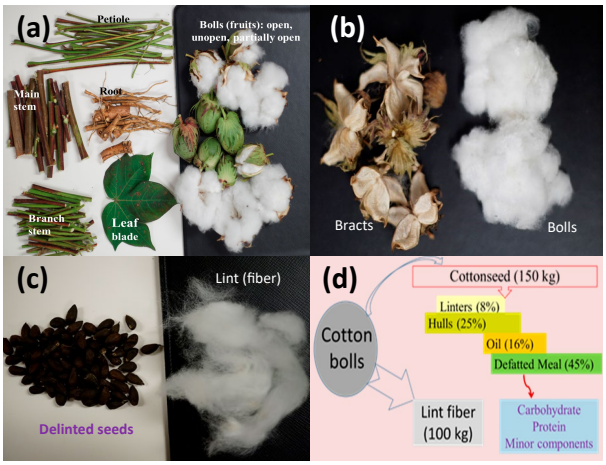

Figure 1. Illustration of cotton biomass components: (a) whole plant, (b) bolls with separated bracts, (c) seeds with ginned linter, and (d) cottonseed composition. Compiled based on Cheng et al. (2020) and He et al. (2020a). Images credited to John Brooks and Haile Tewolde (USDA-ARS, Mississippi State, MS).

Z.He* and Y. Liu, USDA-Agricultural Research Service (ARS), Southern Regional Research Center (SRRC), 1100 Robert E. Lee Blvd., New Orleans, LA 70124.
*Corresponding author: zhongqi.he@usda.gov

Fourier transform infrared (FT-IR) spectroscopy, a nondestructive instrumental technique, used in combination with attenuated total reflection (ATR) sampling is an important tool in cotton fiber (Abidi et al., 2008; Liu et al., 2011; Santiago and Hinchliffe, 2015) and other cotton plant biomass research (Fortier et al., 2015a; He et al., 2018a; Himmelsbach et al., 2006; Liu et al., 2015, 2016). Representative ATR FT-IR spectral characteristics of cotton fiber and cotton plant parts are illustrated in Fig. 2. Overall results have exhibited the sensitivity and availability of FT-IR technique to detect subtle differences between samples that could be neither measured by other procedures nor distinguished visually. In this review, we synthesize and analyze the information from the FT-IR spectroscopic techniques and data analysis used in cotton fiber and cottonseed research.

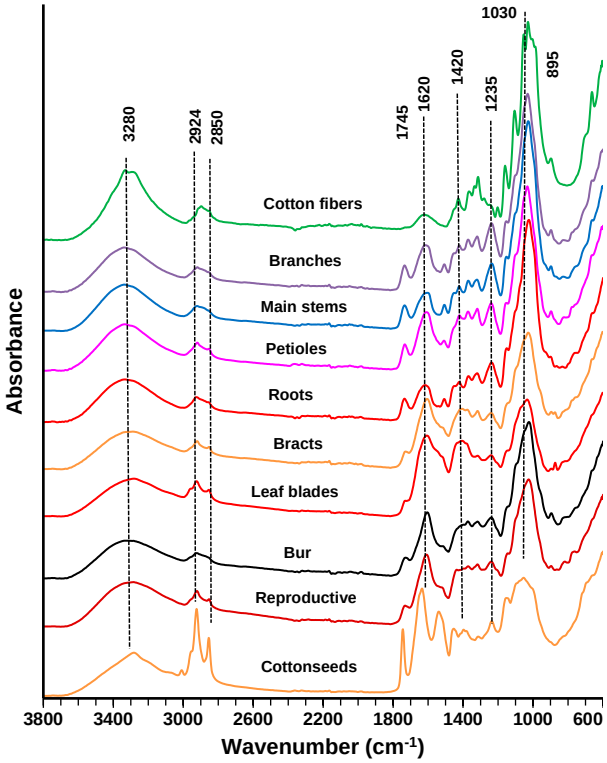

Figure 2. ATR-FTIR spectral features of cotton plant parts and their functional group assignments. Adapted from Liu et al. (2016) with additional bands assignments at 1545, 1420, and 895 cm^{-1}.

FT-IR APPLICATION IN APPLIED COTTON FIBER RESEARCH

FT-IR Evaluation of Fiber Cellulosic Formation. Biosynthesis of cotton fiber cellulose and its biological, chemical, and physical structure understanding has been summarized in many publications (Fang, 2018; Fang and Percy, 2015; Gordon and Abidi, 2017; Gordon and Hsieh, 2007; Wakelyn et al., 2007). Cell wall chemical compositions of cotton fibers at various developmental stages (Fig. 3A) have been analyzed by traditional methods of extraction and separation followed by chemical and instrumental determination. Two typical measuring methods of fiber cellulose content are the anthrone method (Viles and Silverman, 1949) and the Updegraff method (Updegraff, 1969), which use a cellulose standard solution and take at least 2 days to measure cellulose content for each sample mostly due to the slow hydrolysis process of fiber cellulose. Complementary to these chemical analyses, advanced instrumental methods (direct vs. indirect) have been developed to assess fiber cellulose quantitatively or qualitatively as reviewed by Liu (2015). For example, cross-sectional image analysis and ATR FT-IR spectroscopy are direct methods. High volume instrument (HVI^{TM}), advanced fiber information system (AFIS), and Cottonscope® are examples of indirect methods.

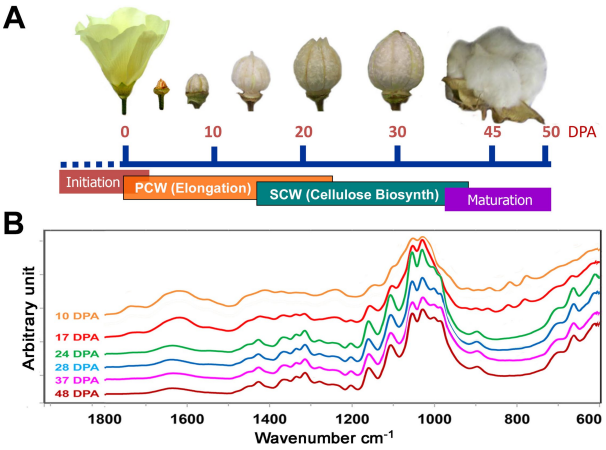

Figure 3. ATR FT-IR spectral monitoring of cotton fiber growth: (A) Cotton boll (flower) formation with days post anthesis (DPA) progression. (B) ATR FT-IR spectral response of TM-1 boll fibers to various DPA. Adapted from Liu and Kim (2017b).

In the past decade, ATR FT-IR spectroscopic method has been used to generate cotton fiber development information (Abidi and Manike, 2018; Abidi et al., 2008, 2010b, 2014; Kljun et al., 2014;

Lee et al., 2015; Liu and Kim, 2015; Liu et al., 2011, 2012; Santiago and Hinchliffe, 2015). An example of ATR FT-IR spectral response to developmental cotton fibers is shown in Fig. 3B. Different spectral interpretation strategies have been used to derive chemical and structural information from ATR FT-IR data. Specifically, direct use of one-band intensities, calculation of two- or three-band intensity ratios, and adoption of chemometrics using principal component analysis (PCA) and partial least square (PLS) analysis are reviewed below. Generally, FT-IR method 1) requires minimal sample preparation by applying the ATR sampling attachment directly on a small bundle of cotton fibers as little as 0.5 mg (nondestructive analysis), 2) is able to analyze samples routinely and rapidly (i.e., less than 2 min for sample loading, spectral acquisition, and subsequent result reporting), 3) is sensitive to fiber chemical and compositional changes reflected by characteristic IR band appearance and shift, and 4) generates multiple parameters from one FT-IR spectrum.

In comparison of the compositional and structural difference between two cotton cultivars (TX19 vs. TX55), Abidi et al. (2010b) analyzed unique ATR FT-IR bands and related their IR intensity variations with the days post anthesis (DPA)-dependent cotton cellulose formation. The authors noted that the TX19 fibers increased linearly in the intensity of the 710 cm^{-1} band (CH_2 rocking vibration in cellulose I_β) from 10 to 30 DPA. In contrast, the TX55 fibers have an intensity change of the 710 cm^{-1} band only at 21 DPA. In addition, analyzed by PCA, the authors reported two groups of spectra (or samples) for each cultivar and enhanced the difference between two cultivars. They observed different transition phases between the two cultivars and further verified the finding with chemical measurements of sugar and cellulose contents by established analytical protocols (Abidi et al., 2010a). Abidi et al. (2014) took a similar approach to compare fiber development in two cotton cultivars [Texas Marker-1 (TM-1) vs. TX55] and reported the usefulness of ATR FT-IR spectral intensities at 3286, 1738, 1639, 1543, 1161, 897, 710, and 667 cm^{-1} to estimate SCW cellulose deposition. The authors correlated the intensities of the bands at 667 and 897 cm^{-1} with the percentage of cellulose determined by the anthrone method and showed a relatively easy way of determining cotton fiber cellulose content. Furthermore, with the same two cultivars, Abidi and Manike (2018) observed a linear relationship between the crystallinity (%) derived from wide-angle X-ray diffraction (XRD) and calculated from either the two-band ratio at 1372 and 2900 cm^{-1} or the single-band integrated intensities of two bands at 667 or 897 cm^{-1}.

In a recent comparative investigation of cellulose crystallinity in two developing cotton cultivars (Upland cotton 0-153 and sea island cotton S-6), Zhang et al. (2020) calculated four different crystallinity index (CI) values from IR bands in four separate regions and found that only the Carrillo-Colom index (i.e., the intensity ratio of 1278 cm^{-1} against 1263 cm^{-1}) showed good correlation with XRD CI values. They also tested the applicability of the developing fiber CI model for estimating CI values of mature fibers. Although a promising result was obtained with randomly selected samples, the authors cautioned that a large number of fiber samples is necessary to ensure an effective model for assessing the crystallinity of mature fibers. Zhang et al. (2021) reported data of cellulose inside the developing cotton fibers obtained from transmittance FT-IR microscopy and ATR FT-IR technique in the high wavenumber range (2800-3000 cm^{-1}). The authors proposed a wax crystallinity index (WCI) for estimating cellulose crystallinity in developmental cotton fibers, from the peak height and area ratios of curve-fitted 2900 cm^{-1} versus 2850 cm^{-1}, and 2900 cm^{-1} versus 2920 cm^{-1}. They noted a good coefficient of determination between the WCI values and XRD CI values.

FT-IR Parameters for Post-Harvest Fiber Quality and Their Implications. Taking a different approach, Liu and colleagues (Liu and Kim, 2015; Liu et al., 2011, 2012) developed alternative algorithms for assessing cotton fiber infrared maturity (M_{IR}), crystallinity (CI_{IR}), and developmental index (or R values) from ATR FT-IR spectral measurement (Table 1). Briefly, M_{IR} calculation consists of two algorithms: the first algorithm ($R_1 = (I_{956} - I_{1500})/(I_{1032} - I_{1500})$) using three IR intensities at 1500, 1032, and 956 cm^{-1} and the second algorithm ($M_{IR} = (R_1 - R_{1,sm})/(R_{1,lr} - R_{1,sm})$ converting R_1 values into fiber M_{IR} with the respective M_{IR} values of 0.0 and 1.0 for the most immature and mature fibers in their dataset (Liu et al., 2011). In the equation, R_1, $R_{1,lr}$, and $R_{1,sm}$ are the respective R_1 values for the unknown sample, the largest R_1 (0.59) and the smallest R_1 (0.14) that were determined from the dataset. The authors validated the efficiency of estimating fiber M_{IR} value from direct ATR FT-IR measurement with cotton fibers of known maturity readings determined from traditional cross-sectional image analysis (IA) and AFIS methods and reported a good agreement between M_{IR} against referenced IA and AFIS maturity readings on selected fiber sets (Liu et al., 2011, 2019).

Table 1. Definition, assessment, and potential implication of three IR indices (M_{IR}, CI_{IR}, and R values)

	M_{IR}	CI_{IR}	R values
Definition & Reference	**IR-based fiber maturity (Liu et al. 2011, 2019).**	**IR-based cellulose crystallinity index (CI) (Liu et al. 2011, 2012).**	**IR-based cellulose biosynthesis (Liu & Kim 2015).**
Calculation[z]	**M_{IR} consists of two algorithms: (1) $R_1 = (I_{956} - I_{1500})/(I_{1032} - I_{1500})$, utilizing 3 IR intensities at 1500, 1032, and 956 cm^{-1}. (2) $M_{IR} = (R_1 - R_{1,sm})/(R_{1,lr} - R_{1,sm})$, converting R_1 values into fiber M_{IR}.**	**CI_{IR} involves two algorithms: (1) $R_2 = (I_{708} - I_{800})/(I_{730} - I_{800})$, utilizing 3 IR intensities at 800, 730, and 708 cm^{-1}. (2) CI_{IR} (%) = $(R_2 - R_{2,sm})/(R_{2,lr} - R_{2,sm})$ x100, converting R_2 values into fiber CI_{IR}.**	**R values are from the equation: $R = (A_{1315} - A_{1800})/(A_{1236} - A_{1800})$, using 3 IR intensities at 1800, 1315, and 1236 cm^{-1}.**
Applications	**• Fiber reference genome research (Kim et al. 2016). • Fiber developmental difference in NILs[y] (Liu & Kim 2019). • Fiber separation of developing vs. developed NILs (Liu & Kim 2020). • Fiber phenotyping (Kim et al., 2019).**	**• Applicability to fibers grown in culture (Liu & Kim 2015). • Assessing cotton cellulose content (Liu & Kim 2017b). • Fiber developmental difference in NILs (Liu & Kim 2019). • Fiber separation of developing vs. developed NILs (Liu & Kim 2020). • Fiber strength (Islam et al. 2016; Liu et al. 2014). • Fiber thermal stability- an indicator of the decomposition of the amorphous cellulose (Nam et al., 2017).**	**• Applicability to fibers grown in culture (Liu & Kim 2015). • Assessing cotton cellulose content (Liu & Kim 2017b). • Fiber separation of developing vs. developed NILs (Liu & Kim 2020).**

[z] Band intensity is measured by relative peak heights at 1500 cm^{-1} for M_{IR}, 800 cm^{-1} for CI_{IR}, and 1800 cm^{-1} for R values.

[y] NILs-near-isogenic lines.

Simultaneously, Liu et al. (2011) proposed an additional algorithm for estimating cotton FT-IR-based fiber crystallinity (CI_{IR}). Such estimation involves two algorithms: the first algorithm ($R_2 = (I_{708} - I_{800})/(I_{730} - I_{800})$) using three IR intensities at 800, 730, and 708 cm^{-1} (Liu et al., 2011) and the second algorithm (CI_{IR} (%) = $(R_2 - R_{2,sm})/(R_{2,lr} - R_{2,sm})$ x100) changing R_2 values into fiber CI_{IR} (Liu et al., 2012). Here, R_2, $R_{2,lr}$, and $R_{2,sm}$ are the respective R_2 values for the unknown sample, the largest R_2 (3.40) and the smallest R_2 (1.40) as reported. The authors noted a strong correlation between CI_{IR} and R_3 (or CI_{XRD}) on a small set of fiber samples and indicated the equivalence and effectiveness of two separate measurements in crystallinity characterization. After measuring the fiber bundle strength via Stelometer instrument and collecting ATR FT-IR spectra on tiny breakage specimens resulting from Stelometer testing, Liu et al. (2014) observed an increase in fiber tenacity (or strength) with CI_{IR} for Pima fibers rather than for diverse Upland fibers. In this approach, the fiber bundles (2 ~ 5 mg) are not enough for a regular XRD scan that requires a large sample (~150 mg on a regular XRD holder of 25 mm diameter x 2 mm deep), whereas these specimens are enough for ATR FT-IR measurement that has microsampling capability. The concept of CI_{IR} values was also adopted as an indicator of the decomposition of amorphous cellulose during evaluation of the thermal stability of mechanically purified cotton fiber (Nam et al. 2017).

Liu and Kim (2015) introduced a third ATR FT-IR algorithm (R values) to detect cotton fiber developmental differences between in planta and in culture. R values are computed from $R = (A_{1315} - A_{1800})/(A_{1236} - A_{1800})$, with the use of three IR intensities at 1800, 1315, and 1236 cm^{-1}. Major bands used in R value algorithm are different from those used in M_{IR} and CI_{IR} algorithms, reflecting different information between R values and M_{IR}/CI_{IR} index. Whereas both the R values and the first principal component (PC1) score increased with fiber DPA, the R values detected subtle differences between fiber older than 25 DPA grown in planta against in culture compared to PC1 score.

For verification and application of these FT-IR-based indicators of cotton fiber, Liu and Kim (2015) demonstrated the capability of the three IR indices (M_{IR}, CI_{IR}, and R value) in monitoring the

phase transition from PCW to SCW biosynthesis and also in revealing the difference in the phase transition between two types of fibers grown in planta versus in culture. The authors found that the *R* value algorithm could be more effective than PCA in differentiating between the developing fibers (> 25 DPA) grown in planta and those in culture. As cotton fiber is available in large quantities in field production, sampling quantity is generally not a concern for routine fiber analysis in cotton industry. However, there is a limited amount of cotton fibers grown in culture for research; an ATR sampling device with FT-IR would facilitate the rapid and nondestructive characterization of cotton fiber. To better understand the cotton reference genome and phenotype, Kim et al. (2016) measured fiber and seed properties from multiple *Gossypium raimondii* Ulbrich lines with physical and analytical tools that included ATR FT-IR for fiber M_{IR} assessment. The authors reported lower M_{IR} values for three available *G. raimondii* accessions than those for Upland fibers examined (TM-1, SA-1, and SA-481), and ascribed a small M_{IR} value for green SA-481 fiber to the green trait that could affect cellulose deposition in plants. Further, after comparing M_{IR} values of 80 F2 plants with various fiber maturities among their genotypes, Kim et al. (2019) showed a match between M_{IR}-based phenotypes and DNA marker-based genotypes as well as between M_{IR}-based phenotypes and both micronaire and lint percentage-based genotypes. Such a match would offer an alternative means for cotton biologists/geneticists to screen fiber maturity rapidly and efficiently. In research of the cotton biosynthesis mechanism, Kim et al. (2013a, b) found an immature fiber (*im*) mutant with unique characteristics of non-fluffy cotton bolls, a thin SCW, and less mature fibers compared to its near-isogenic line (NIL) wild type TM-1. Liu and Kim (2017a) did not find an inherent difference between developmental TM-1 and *im* fibers (12 to 44 DPA) after PCA and simple algorithm interpretation of ATR FT-IR spectra. However, they reported the difference in normalized intensity variations of the 730 cm^{-1} band between two types of fibers: the 730 cm^{-1} band intensities in developmental *im* fibers are observed to be lower than those in developmental TM-1 fibers, whereas these intensities in fully mature TM-1 and *im* fibers are close. Liu and Kim (2017b) linked the cellulose content determined by chemical analysis to ATR FT-IR indices acquired by the reported procedures, and found that CI_{IR}, *R* value, and the integrated intensity of the 895 cm^{-1} band exhibit strong and linear relationships with cellulose content within developmental TM-1 and *im* fibers.

In an in-depth study of the effect of genetics and crop year on cotton fiber cellulose biosynthesis, Liu and Kim (2019) examined M_{IR} and CI_{IR} indices from two pairs of cotton developmental NILs (TM-1 vs. *im* that differ in fiber maturity and MD52ne vs. MD90ne that varies in fiber strength). Their results showed a significant difference in M_{IR} values between developmental TM-1 and *im* NILs in crop year 2015, and a significant difference in CI_{IR} values between these NILs grown at the same field in crop year 2011. Also, the *im* fibers tend to have more CI_{IR} development than the TM-1 fibers when they show close M_{IR} values. In comparison, MD52ne versus MD90ne NIL pair revealed insignificant differences in the patterns of CI_{IR} and M_{IR} as well as the relationship between CI_{IR} and M_{IR} values. These observations are consistent with Islam et al. (2016), who reported that the strengths of developmental fibers increased with CI_{IR} measured with the two NILs.

Liu and Kim (2020) tried to distinguish underdeveloped NIL fibers from developed (matured) NIL fibers by the three FT-IR indicators. The underdeveloped (immature) fibers were collected from 20 to 40 DPA unopened bolls, and mature fibers were harvested after cotton bolls naturally opened (approximately 42 DPA). The PC1 score and *R* values of the two types of samples could be categorized to their own groups (Fig. 4A). These parameters can be used to discriminate underdeveloped from developed fibers. However, there were some overlaps in the M_{IR} and CI_{IR} plots between the two types of samples (Fig. 4B), indicating that a single use of M_{IR} or CI_{IR} index could not classify underdeveloped from developed fibers effectively although their combination improved a separation of NILs (TM-1 vs. *im*) within underdeveloped or developed fibers. A recent study of the cotton fibers of six phenotypes differing in the fiber length supported the argument (He et al., 2021c).

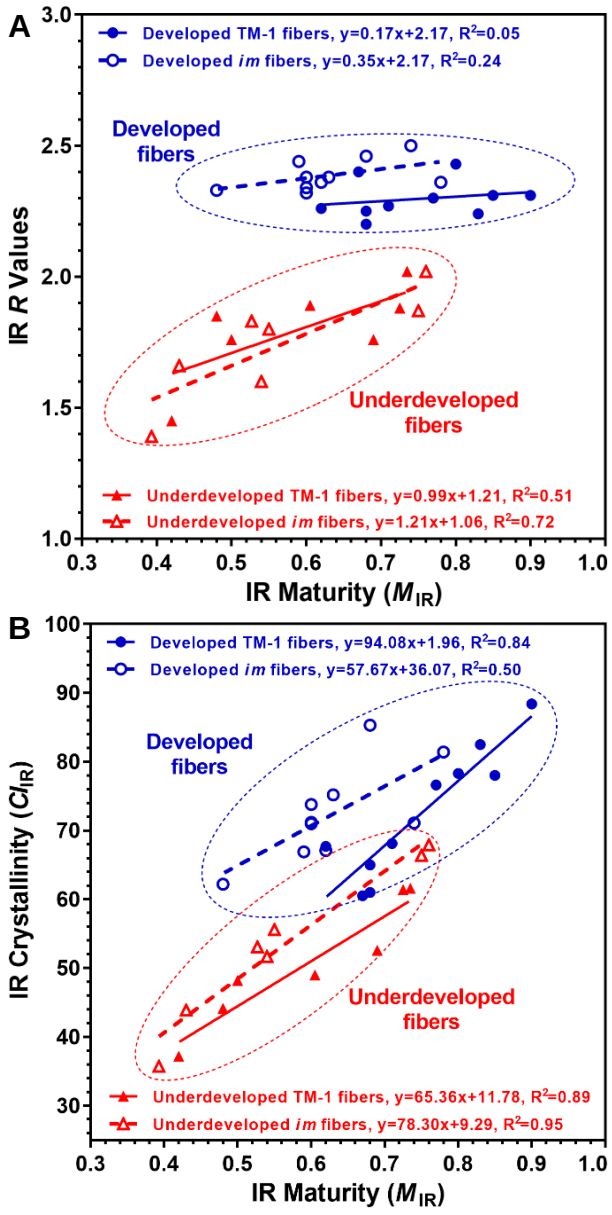

Figure 4. Analysis of the relationship between different IR parameters of underdeveloped fibers: (A) *R* values versus M_{IR} index. (B) CI_{IR} versus M_{IR} index. Pairs of TM-1 and *im* NIL cotton plants were grown side by side in 2007, 2011, 2014, and 2015. Adapted from Liu and Kim (2020).

FT-IR Coupled with Microimaging Techniques for Cotton Fiber Cellulose Development and Contaminant Identification. A combination of conventional one-dimensional IR spectral information and spatial information IR imaging method has been used to study cotton fibers at single fiber level (Church and Woodhead, 2017; Himmelsbach et al., 2003; Santiago et al., 2016, 2017; Wang et al., 2006). The spectral changes observed from FT-IR microspectroscopy/imaging measurement generally are consistent with those observed with macroscopic sampling FT-IR (Santiago et al., 2016, 2017). Furthermore, PCA scatter plot of the microspectroscopy/imaging data distinguishes cotton fibers at different developing phases. One advantage of the microspectroscopy method was to derive the chemical distribution maps that visually can depict general spectral changes (Santiago et al., 2017). Liyanage and Abidi (2019) applied FT-IR microspectroscopy imaging in the transmission mode to investigate changes in cellulose distribution of individual cotton fibers harvested at different stages of fiber development. The authors indicated the usefulness of IR vibrations of cellulose at 897, 1161, and 1429 cm^{-1} in generating cellulose distribution in intact cotton fibers. In addition, FT-IR microspectroscopy is used in characterization of other cotton biomass, such as cottonseed coat (Yan et al., 2009).

Because cotton contaminant occurrence has been a persistent concern in the cotton industry, multiple chemical and physical methods have been developed to measure and identify cotton contaminants (Hequet and Abidi, 2006; Himmelsbach et al., 2006). Abidi and Hequet (2007) demonstrated the feasibility of ATR FT-IR to detect the presence of trehalulose (the dominant sugar in the whitefly honeydew residue). The authors reported that the integrated intensities of the peaks located at 3280, 1622, and 1018 cm^{-1} show high correlation with trehalulose content. In addition, they suggested the possibility of implementing PCA to discriminate the ATR FT-IR spectra of contaminated from that of noncontaminated cotton fibers. Recently, Fortier et al. (2015a, b, 2017) applied ATR FT-IR spectroscopy and microspectroscopy imaging to identify botanical and field cotton trash. The authors reported that botanical trash was identified independently from cotton fibers even though both contained cellulose, and field trash and botanical trash were easily identified due to their differences in chemical makeup.

Non-cellulosic impurities in outermost layers of cotton fiber contribute to the hydrophobic feature in gray cotton fabrics. Dave et al. (2014) treated the fabrics with air dielectric barrier discharge and examined the treated fabrics by ATR FT-IR and scanning electron microscopy (SEM). The results showed that the treatment improves wettability of gray cotton due to the removal of non-cellulosic impurities (characterized by the weaking 2852 and 2918 cm^{-1} bands of hydrophobic alkyl group) and the formation of polar carboxylate group (indicated by a strong carboxyl peak at 1749 cm^{-1}). In addition, the authors noted a good agreement in measuring morphological changes

between ATR FT-IR and SEM methods. The ATR FT-IR approach offers a fast and satisfactory assessment of removal of impurities from cotton fiber surface when they were treated or modified.

FT-IR CHARACTERIZATION OF COTTONSEED PRODUCTS

FT-IR Monitoring of Cottonseed Oil Structural Changes Impacted by Processing and Application Factors. In oil crushing, cottonseed is processed into two major products: cottonseed oil (CSO) and defatted cottonseed meal (CSM) (Fig. 1). FT-IR spectral analysis clearly shows the separation as the spectral features of the whole cottonseed are more like the combination of those of CSO and CSM (Fig. 5). The multiple peaks or shoulders around 2922 cm^{-1}, an indicator of the high hydrophobicity or low wettability of the testing sample, are strong in the oil's spectrum as CSO is dominated by the aliphatic CH_3 and CH_2 groups of triglycerides. FT-IR spectroscopy has been used for the qualitative and quantitative comparison of edible oils (Kaur et al., 2019). Arslan et al. (2019) reported the FT-IR and fingerprint spectra of 40 different types of pure vegetable oils, such as those from black cumin seed, sunflower, hazelnut, cottonseed, soybean, and olive. Those FT-IR spectra collected from 4000 to 650 cm^{-1} appeared quite similar, with no unique peaks even in the fingerprint region (1600-650 cm^{-1}). Thus, it is necessary to apply multivariate classification models with the spectral data for determining the types of refined vegetable oils. FT-IR spectroscopy could provide useful information of CSO as some band intensities of FT-IR spectra highly correlate with the chemical properties of CSO, such as iodine value (IV), saponification value (SV), peroxide value (PV), free fatty acids (FFA), and induction period (IP) (Shah et al., 2017). Specifically, the band at 721 cm^{-1} is correlated with SV and the bands at 1161 and 1743 cm^{-1} with IP. The band at 2852 cm^{-1} is linked to the PV of CSO, whereas the band at 3009 cm^{-1} is associated with the IV of CSO and the band of carbonyl at ~1709 cm^{-1} for the determination of FFA. These matching relationships would provide a quality check for variations in the physiochemical properties of cottonseed varieties (Shah et al., 2017). Using FT-IR, Mahesar et al. (2017) quantified FFA content in crude oil from different cottonseed varieties in Pakistan. The authors presented typical FT-IR spectra of two CSOs with low and high FFA contents. The authors reported that both CSO spectra are comparable so the spectral features can be correlated with the main components of edible oils, specifically triacylglycerol. However, there is a considerable difference between both spectra in terms of peak intensity, in particular at 1710 cm^{-1}. Thus, FT-IR coupled with PLS and PCA regression models were used to develop calibrations in the specific absorption region of carbonyl between 1690 and 1727 cm^{-1}. Their work indicated that the component analysis-coupled FT-IR could be used as a greener alternative to the standard titration method. Similarly, Talpur et al. (2014) applied single-bounce (SB) ATR FT-IR in conjunction with chemometrics for accurate determination of FFA, PV, IV, conjugated diene (CD), and conjugated triene (CT) of CSO. Their results showed that this FT-IR spectroscopic analysis coupled with multivariate chemometric techniques could be applied for the fast and simultaneous determination of the five parameters in frying CSO and other vegetable oils.

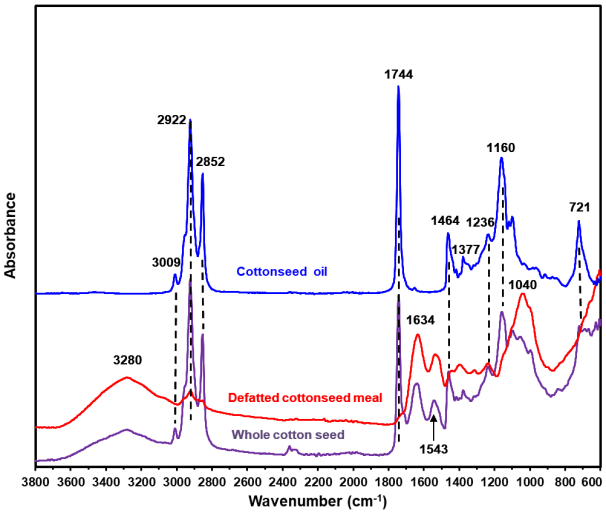

Figure 5. ATR FT-IR spectra of whole cottonseed, and its major components of cottonseed oil and defatted cottonseed meal.

As an unsaturated oil, CSO has a ratio of 2:1 of polyunsaturated (65-70%) to saturated fatty acids (26-35%) (Gaddam and Palanisamy, 2017). The unsaturated fatty acids consist of 18 to 24% oleic and 42 to 52% linoleic and linolenic acids. High degree of unsaturation of CSO provides possibilities for chemical transformation leading to functionalized oligomers and polymers. Jia et al. (2011) synthesized cottonseed oil-based polyol with sorbitol derived from natural source and characterized the chemical structure of the products with FT-IR analysis. The polyol was prepared by ring-opening of the epoxidized CSO with sorbitol. Differences in FT-IR spectra among 1) CSO, 2) epoxidized CSO, and 3) CSO-based polyols were

obvious. In the spectrum of epoxidized CSO, the band related to C=C double bonds from CSO at 3008 cm^{-1} disappeared, and new epoxy-related doublet peaks at 823 and 843 cm^{-1} appeared. This observation indicated the C=C functional groups in CSO were turned into epoxy groups. After the ring-opening reaction, the characteristic peaks of epoxidized CSO weakened and a hydroxyl band at approximately 3467 cm^{-1} became prominent. Similar FT-IR spectral changes also were observed in conversion of CSO into a polymerizable polyol by in-situ epoxidation and hydroxylation in the presence of water as nucleophile and sulfuric acid as catalyst (Narute and Palanisamy, 2016), and in synthesis of eco-friendly polyester polyols by the condensation reaction of epoxidized CSO and polyethylene glycol (Gaikwad et al., 2015). Kurtulbaş et al. (2018) assessed lipid oxidation in CSO treated with phytonutrients (200 ppm of gallic acid, rutin, tertbutyl hydroquinone, or β-carotene). The authors compared the FT-IR spectral features of pure and treated CSOs. The authors did not find a difference between the two types of samples, assuming that the concentration of these additives was not high enough to be detectable in the FT-IR spectra.

Meshram et al. (2013) prepared and characterized CSO-based polyesteramide for coating applications. The authors applied multiple spectral techniques including FT-IR to analyze the base-catalyzed aminolysis of CSO and incorporation of vinyl acetate into the final products. The fatty acid constituents (C=C stretching) in fatty amide were observed at 1622 cm^{-1}. The FT-IR bands at 1732 and 1599 cm^{-1} of the final product (modified CSO polyesteramide) supported the presence of vinyl acetate/ester amide and unsaturation. In addition, a new characteristic peak appeared at 796 cm^{-1} of the final product, attributed to the CH vibrations of vinyl groups. Gaddam and Palanisamy (2017) synthesized vegetable oil-based waterborne polyurethane-imide dispersions using maleated CSO polyol as ionic soft segment. FT-IR characterization indicated the incorporation of imide functionality in the film backbone shown by the imide-I and II bands at 1777 and 1370 cm^{-1}, in comparison to the spectral features of untreated CSO.

FT-IR Characterization of Cottonseed Protein Structures and Its Interaction Mechanisms with Additives in Product Formations. Protein is a major component in cottonseed with mutiple polypeptides (i.e., various protein fractions) used for storage or biological functions (He et al., 2018b; Singh and Kaur, 2019). After oil crushing, the protein component is retained in defatted CSM and protein isolate products. In the FT-IR spectra of protein samples, the bands at 1653, 1532, and 1236 cm^{-1} could be attributed to amide I (C=O stretching), II (CN stretching, NH bending), and III (CN stretching, NH bending) bands of proteins, respectively (Chen et al., 2013). In addtion, Yue et al. (2020) included N–H bending and O–H stretching vibrations at 3295 cm^{-1} and helix structure in amide III at 1060 cm^{-1}. The authors observed no changes of FT-IR peak positions with cottonseed products with 50 and 74% protein content, suggesting that the concentration treatment had no obvious effect on the functional groups of cottonseed protein. Indeed, these FT-IR features have been applied to study cottonseed protein-rich samples (He et al., 2014a). These protein-related IR bands at 1653, 1532, and 1236 cm^{-1} are basically the same among the four samples examined (Fig. 6). However, differences in the band intensities at 1448 and 1398 cm^{-1} were observed between these samples. The relative height of the band at 1398 cm^{-1}, compared to that at 1448 cm^{-1}, was lower in water-washed cottonseed meal (WCSM), phosphate buffer-washed cottonseed meal (BCSM), and cottonseed protein isolate (CSPI) than in CSM, indicating differential removal of some of these compounds during the preparation of WCSM, BCSM, and CSPI from the raw material CSM. The broad band at 1070 cm^{-1} could be assigned mainly to carbohydrate, a major component in cottonseed products. The authors reported the relative band areas as 85.5, 60.5, 65.3, and 15.8, respectively, for CSM, WCSM, BCSM, and CSPI. The content of carbohydrate was high in CSM, approximately same in WCSM and BCSM, and less in CSPI.

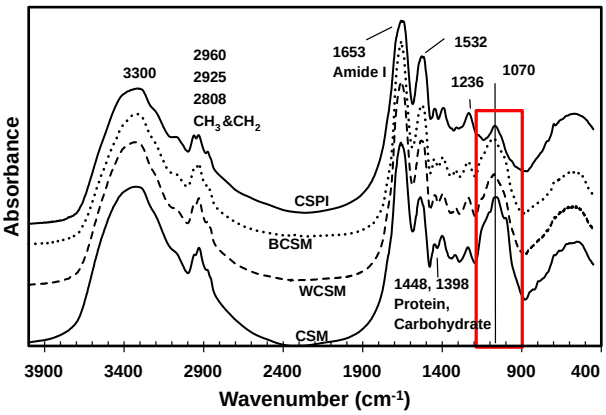

Figure 6. FT-IR spectra of defatted cottonseed meal (CSM), water-washed CSM (WCSM), phosphate buffer-washed meal (BCSM), and protein isolate (CSPI). The peak area indicated by red rectangle is used to calculate the relative content of carbohydrate in these samples. Adapted from He et al. (2014a).

FT-IR characterization of whole cottonseed protein CSPI and its two fractions (i.e., water soluble CSPw and alkali soluble CSPa isolates) was also reported (He et al., 2013). The intensties of the three bands at 1309, 1173, and 926 cm^{-1} in the spectrum of whole CSPI are between those of water soluble CSPw and alkali soluble CSPa fractions as both protein fractions comprise the whole CSPI. The minor peak at 1309 cm^{-1} was observd in the spectrum of alkali soluble CSPa, but was not obvious in that of water soluble CSPw, indicating some structural difference between the two fractions of cottonseed protein. In contrast, a small peak at 1173 cm^{-1} and a shoulder band at 926 cm^{-1} were observed in the spectrum of CSPw, attributed to phytate compounds (He et al., 2006)sXml. This assignment is supported by elemental analysis that showed P content approximately four times higher in CSPw than in CSPI and CSPa (He et al., 2015).

Furthermore, deconvolution of relevant FT-IR spectral band of the amide I (1600-1700 cm^{-1}) envelope can be used to calculate the secondary structural features of these proteins (Table 2). This approach designated the α-helix structure to 1649 to 1660 cm^{-1}, the random coil structure to 1638 to 1648 cm^{-1}, the β-sheet structure to 1606 to 1637 cm^{-1} and 1670 to 1680 cm^{-1}, and β-turn structure to 1660 to 1700 cm^{-1} minus 1670 to 1680 cm^{-1} (Zhao et al., 2008). The relative distribution of the secondary structures in all cottonseed protein samples were β-sheet (~40%) > β-turn (~33%) > α-helix (~14%) > random coil (~12%). Similar to the qualitative visual observation of FT-IR spectra, differences in the secondary structures between CSPw and other protein isolates were observed, reflected in higher α-helix and lower β-sheet contents of CSPw. Those observations were consistant with results obtained from other advanced instrumental characterization (He et al., 2018c). Li et al. (2017) compared the FT-IR spectral features of pilot-produced WCSM obtained by different drying methods (oven, freeze dryer, and spray dryer). The authors found that the band around 1050 cm^{-1} in the pilot-produced WCSM samples was much stronger than that of lab-produced WCSM samples. The authors attributed the difference to the contribution of cotton fiber residues (i.e., carbohydrate components) in the meal products as more crude fibers were in the pilot meal raw material than that the defatted raw meal used for lab production, although the FT-IR spectra showed no impact of the drying method on the fiber component and the whole spectral features.

Cottonseed protein-based products have shown promise as sustainable bio-based wood adhesives (He and Cheng, 2017). Comparison of the differences in the FT-IR features of cottonseed protein products provided insight on the adhesive mechanisms. Pradyawong et al. (2018) blended CSM products with different protein contents to evaluate cost-effective wood adhesives. The FT-IR profile of the sample with 94.8% protein content showed slightly broader peaks of amide II and III at 1524 and 1233 cm^{-1}, compared to those of samples with 34.9 and 46.3% protein content, respectively. Furthermore, the authors observed the absence of the 1393 cm^{-1} band and the presence of a new band at 1316 cm^{-1} of the two samples with low protein content. Based on the observation, the authors proposed cross-link interactions occurred between protein group (ε-NH2) and carbohydrate aldehyde group.

Cheng et al. (2019) obtained the FT-IR spectra of CSPI with nanocellulose. The authors found that the amide I band was shifted from 1631 cm^{-1} of CSPI to 1635 cm^{-1} of the adhesive of CSPI mixed with 10% cotton nanocellulose (CNC). The authors attributed the 4 cm^{-1} shift to the hydrogen bonding formation between the protein amide group and cellulose

Table 2. Purity and secondary structures of cottonseed and soy protein isolates. Data are presented in average ± standard deviation (n = 4). Values with a same letter in the same column of all protein isolates are not statistically significant (p = 0.05) between the protein isolates. Adapted from He et al. (2013)

Sample[z]	Purity (% of dry matter)[y]		Secondary structures (% of total structure)			
	N analysis	Color	α-Helix	β-Sheet	β-Turn	Random coil
CSPI	**95.3 ± 1.7a**	**78.0 ± 2.1a**	**13.4 ± 0.3a**	**41.4 ± 0.9a**	**33.2 ± 0.5a**	**11.9 ± 0.2a**
CSPw	**85.8 ± 3.1b**	**96.2 ± 4.3b**	**14.3 ± 0.2b**	**40.2 ± 0.5b**	**33.5 ± 0.2a**	**12.0 ± 0.2a**
CSPa	**108.6 ± 1.5c**	**104.0 ± 8.8b**	**13.5 ± 0.1a**	**41.2 ± 0.4a**	**33.2 ± 0.2a**	**12.1 ± 0.1a**
SPI	**90.5 ± 1.3d**	**80.2 ± 3.9a**	**13.4 ± 0.4a**	**41.4 ± 1.3ab**	**33.2 ± 0.7a**	**12.0 ± 0.2a**

[z] CSPI and SPI are whole cottonseed and soy protein isolates. CSPw and CSPa are water and alkali soluble cottonseed protein isolates (fractions).

[y] Protein purity was compared based on two methods (i.e., total N analysis and protein coloric measurement).

hydroxy groups. Such a hydrogen bonding could enhance the compatibility between the protein and the nanocellulose components. Similarly, Li et al. (2019) examined the FT-IR spectra of phosphorus/calcium-cottonseed protein adhesives. The amide I, II, and III bands of modified CSPI adhesives had significantly decreasing peak intensities and red-shift phenomena. The secondary structures of cottonseed protein were changed after blending with these phosphorus/calcium reagents. FT-IR spectroscopy was applied to characterize "greener" adhesives composed of urea-formaldehyde resin (UF) and WCSM (Liu et al., 2018). The researchers observed FT-IR spectral features typical for both UF and WCSM, but no new absorption peaks appeared. Thus, any possible chemical connections between WCSM and molecules of UF resins needs to be verified. Chen et al. (2020) examined the FT-IR spectra of the adhesives of defatted CSM mixed with polyamine-epichlorohydrin resin. The authors noticed a new shoulder band at 1730 cm^{-1} (ester C=O bonds) in the spectrum of the cured adhesive, compared to uncured sample. However, the authors did not elaborate on this observation. A more recent work (He et al., 2021a) reported a status quo way to examine the CSPa and CSPw adhesive bonding performance. The authors placed the cohesive-broken bonding surface of the glued wood pairs directly on the ATR probe for FT-IR spectroscopic analysis. The spectra showed the difference in the band shape around 2926 cm^{-1} between CSPw and CSPa adhesives. As the band features at 2926 cm^{-1} are related to wettability (or hydrophobicity), the observation confirmed the different hydrophobicity or wettability between the two cottonseed protein adhesives, and suggested the wettability of cured cottonseed protein adhesives is an important factor to determine the interaction on adhesive-wood bonding.

In addition to cottonseed protein-based wood adhesive research, CSPI also has been used as a paper additive (Cheng et al., 2017). The spectra of papers with CSPI treated with 11% protein solution showed two prominent peaks at 1640 and 1530 cm^{-1}, corresponding to the amide I and II bands, respectively, and a weaker peak at 1260 cm^{-1} corresponding to the amide III band. In the spectra for paper with CSPI and an acid (e.g., 200 mM citric acid), the intensities of the amide peaks decreased relative to the cellulose peaks. The authors concluded that the presence of the acid appears to allow cottonseed protein to better penetrate the paper. In comparison of the spectra of cottonseed protein bioplastics, Yue et al. (2012) reported a new peak centered at 1665 cm^{-1} for cottonseed protein bioplastic products, and attributed it to the imine (–CH=N–) stretching vibration from cross-linking of the two components. Chen et al. (2019) prepared a series of bio-based packaging films from cottonseed protein and poly (vinyl alcohol) (PVA) modified with different plasticizers. The authors detailed the FT-IR spectral changes of the CSPI/PVA blend films with a weight ratio of 3:7 in references to CSPI and PVA alone and impacted by plasticizers. The FT-IR band intensity (area) associated with the β-sheet showed a decreasing trend in the amide I band of the blend film after the addition of plasticizers, whereas there was an increase in the band area associated with the β-turn structure. The authors attributed the observations to plasticizers gradually inserted into the CSPI β-sheet structure generated hydrogen bond interactions, increasing the free volume of the peptide chain. Plasticizer insertion, therefore, gradually weakens or even breaks the hydrogen bond interactions between the β-sheet layers, resulting in a gradual shift in the β-sheet to a β-turn. An increase in β-turn structures would be beneficial as it improves the flexibility of the CSPI-based films. Zhang et al. (2010) prepared CSPI-based superabsorbent hydrogel by graft copolymerization of hydrolyzed cottonseed protein and acrylic acid monomer. FT-IR analysis found new absorption band at 1687 cm^{-1} in the hydrogel, which was assigned to the C=O stretching of the amide bands. Furthermore, the authors contributed it as the characteristic of the CONHR group in the polypeptide of cottonseed protein. Thus, the comparison of the FT-IR spectra confirmed the grafting copolymerization of acrylic acid monomer onto the hydrolyzed cottonseed protein backbone.

FT-IR Characteristics of Cottonseed Hull. Cottonseed hull is the outer covering of cottonseeds that is removed from the cotton kernel before the oil is extracted (Fig. 1). Silwal et al. (2017) conducted FT-IR analysis of the hull and kernels (inner meats) of delinted cottonseed from two parents (TM-1 and 3-79) and their 17 progeny (chromosomal substitution) lines. The authors assigned band areas in the region of 1700 to 1750 cm^{-1} for lipid, and the regions of 1665 to 1680 cm^{-1}, 1646 to 1660 cm^{-1}, 1638 to 1645 cm^{-1}, and 1615 to 1637 cm^{-1} for four secondary protein structures (respectively, β-turns, α-helices, random coils, and β-sheets) just like those of protein isolates reviewed above. Wavenumbers ranging from

1731 to 1750 cm^{-1} were selected to detect hydrated type of lipids and 1700 to 1730 cm^{-1} were used for the dehydrated types. Based on the FT-IR difference between hydrated and dehydrated lipids in cottonseed hulls as well as kernels, the authors identified two progeny lines with lipid moisture content and protein secondary structures similar to both parents, and three progeny lines remained distinct from either parent. Three were similar to TM-1 parent for lipid and protein profiles, whereas three were comparable with 3-79 parent. These findings would be helpful information in selecting candidate cotton lines as sources of food and feed in breeding programs.

Liu et al. (2015) examined and compared the unique FT-IR bands between five agricultural byproducts (including cottonseed hull) (Fig. 7). Except for a distinctive band at 1740 cm^{-1} (carboxyl C=O groups) with pecan shell, the spectral features of cottonseed hull, pecan shell, and almond shell were similar, indicating their similar lignocellulosic composition. The spectrum of broiler litter is more complicated as broiler litter is a mixture of poultry excreta, spilled feed, feathers, and bedding materials such as wood shavings, sawdust, and peanut hull (Guo et al., 2012). The spectral signature of lignin shows significant C-O groups (due to an intense 1025 cm^{-1} band) but less amide and C=O groups (due to weak bands in the 1800-1600 cm^{-1} region) as the "lignin" residue contains roughly 49.5 wt% of sparingly water-soluble cellulose crystals, 42.1 wt% lignin, and 8.4 wt% extractives (Uchimiya et al., 2013). Liu et al. (2015) further characterized the FT-IR spectral response of these byproducts to differing pyrolysis temperatures and developed a simple three-band algorithm (*R* readings) per the multipoint averages of the band intensities at respective range of 1750 to 1500 cm^{-1}, 2000 to 1790 cm^{-1}, and 645 to 655 cm^{-1} for semi-qualitative comparison of biochar formation. Although Liu et al. (2015) did not report any clear correlations between the *R* reading and pyrolysis temperature of the four types of plant biomass biochars they generated, a recent work (He et al., 2021b) computed the *R* readings of the seven CSM-based biochars prepared at pyrolysis temperatures from 300 to 600 °C. They found the simple *R* readings of the biochars linearly related to the pyrolysis temperature, indicating pyrolysis temperature as a key factor affecting the readings. Uchimiya et al. (2013) analyzed the first derivatives of ATR FT-IR spectra of these five feedstocks and their biochars. The authors found that the free OH peak at 3675 to 3700 cm^{-1} increased by pyrolysis of plant biomass (almond shell and cottonseed hull) at 350 °C, and then dramatically decreased at 500 to 600 °C. Similar changes were also observed with carboxyl C=O stretching vibration at 1650 to 1750 cm^{-1}. That is, the carboxyl C=O peak increased by pyrolysis of almond shell and cottonseed hull at 350 °C, and then dramatically decreased at 500 to 650 °C.

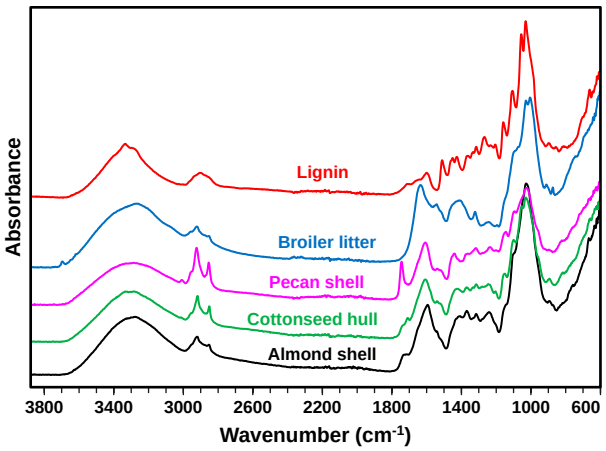

Figure 7. ATR FT-IR spectral comparison of different agricultural byproducts. Adapted from Liu et al. (2015).

Zhou et al. (2016) reported the FT-IR spectra of cottonseed hull, extracted cellulose and cellulose nanofibers (CNFs), rod-like cellulose nanocrystals (CNCs), and spherical cellulose nanocrystals (SCNCs). The authors observed prominent peaks at 1723, 1507 and 1250 cm^{-1} in the spectrum of the raw cottonseed hull, but not in the spectra of other products. This observation indicated that most of the hemicellulose and lignin were removed from the raw cottonseed hull during the preparation of the cellulose and nanofibers. No significant differences were observed in the spectra between the extracted cellulose and nanofibers (i.e., CNFs, SCNCs, and CNCs), suggested that the cellulose molecular structure remained unchanged during the preparation of these nano materials. One exception was the observation that a tiny peak at 1205 cm^{-1} related to SO vibration appeared in the spectra of CNCs due to the esterification reaction that occurred in the sulfuric acid hydrolysis process. Later, FT-IR spectral changes further confirmed the grafting of maleic anhydride onto the surface cellulose nanocrystals from cottonseed hull (Zhou et al., 2018).

Zhou et al. (2011) reported the FT-IR spectrum of spent cottonseed hull after used as substrate for white rot fungus cultivation. Their FT-IR results

revealed the presence of functional groups such as –NH, –OH, C=O, and CONHR in spent cottonseed hull. The authors assumed that these functional groups were potential adsorption sites for interaction with a cationic dye when the spent cottonseed hull was used a low-cost biosorbent to remove this dye from aqueous solution.

CONCLUSIONS AND FUTURE RESEARCH

FT-IR spectroscopy has been one of the power tools for meeting diversified research and development needs of cotton industry. The current trend of FT-IR application in cotton fiber research is mainly on developing quantitative parameters/algorithms to monitor and evaluate the fiber formation in growth and post-harvest quality control. Advancement in this area was reached in last decade as reviewed in the paper. However, the sampling methods can impact FT-IR results (Durak and Depciuch, 2020). Indeed, Ling et al. (2019) reported that some proposed indicators of crystallinity index measured by FT-IR were not in good agreement with their results when the authors evaluated the effects of ball milling on cotton cellulose structures. Thus, cross examination of the FT-IR-based parameters of same fiber samples by multiple laboratories would facilitate data comparison and promote the applicability of the relevant FT-IR model tools from lab research to "real world" testing services. In this regard, cheap, portable, and hand-held FT-IR instrument could be attempted for further applications.

In cottonseed research, FT-IR has been used qualitatively for monitoring band intensity changes and band position shifts. Such information provides evidence and insight on identities and interactions of various functional groups impacted by processing and environmental conditions. Relevant FT-IR data reviewed in this paper indicate that cross-linking is a major mechanism in improving the performances of cottonseed oil, protein, and hull products. Currently, cottonseed protein-enriched products have not been used as food or food additives due to the presence of toxic gossypol in common glanded cotton (Cheng et al., 2020; He et al., 2015). Research efforts have been made for eliminating gossypol from cottonseed to mitigate the toxic effects of gossypol in glandless cottonseed for approval by FDA for food and feed use (He et al., 2021d; Rathore et al., 2020). FT-IR spectroscopic technique would be a low-cost, meaningful tool for structural characterization of the glandless cottonseed protein, its hydrolysates, and active peptides for food applications (He et al., 2020b; Ma et al., 2018; Song et al., 2020).

Currently in cotton research, the major sampling method is the use of ATR device for reflectance FT-IR spectra and traditional KBr pellet for transmittance FT-IR spectra. It should be noted that the penetration depth of ATR-FTIR beam in the cellulose sample was no more than 2 μm, estimated between 0.9 and 1 μm at 2000 cm^{-1} (Kramar et al., 2018; Pereira et al.; 2005). Because the thickness of the SCW in mature cotton fibers is more than 4 μm, ATR FT-IR technique might not be capable of providing full information inside the cotton fibers, especially in the SCW thickening and maturation stages. FT-IR microspectroscopy with transmission mode appears better than ATR FT-IR to acquire more information of cellulose inside of the developing cotton fibers, especially in the high wavenumber region of 2800-3000 cm^{-1} (Liyanage and Abidi, 2019; Zhang et al., 2021).

Alternative approaches for practical needs in cotton-related research could be worth exploring. For example, FT-IR photoacoustic spectroscopy (FT-IR PAS) can eliminate some of the shortcomings of traditional FT-IR caused by scattering effects and reflection issues (Bekiaris et al., 2015; He et al., 2011). This technique is a combination of FT-IR and a photoacoustic detector. The detecting signal is generated by the interaction of the infrared beam with the surface of the sample, which leads to the production of a heatwave that can be detected by a sensitive microphone and transformed into a regular absorption spectrum. Bekiaris et al. (2020) compared 11 bioorganic samples with three FT-IR techniques (diffuse reflectance, PAS, and ATR). The authors found that, although ATR FT-IR provided the best spectra for soft samples, FT-IR PAS is the best technique, providing a greater amount of information. The application of FT-IR PAS in cotton research is in a beginning phase (Church and Woodhead, 2017). The FT-IR PAS method was used to screen raw cotton for variations in wax composition per the alkyl functional groups at the bands near 2900 cm^{-1}. Future research should be conducted with different cotton biomass components to judge the PAS FT-IR method's universal applicability and advantages to applied cotton research.

ACKNOWLEDGMENTS

This work was supported by the U.S. Department of Agriculture, Agricultural Research Service. Mention of trade names or commercial products is solely for the purpose of providing specific information and does not imply recommendation or endorsement by USDA. USDA is an equal opportunity provider and employer.

REFERENCES

Abidi, N., and E. Hequet. 2007. Fourier transform infrared analysis of cotton contamination. Text. Res. J. 77:77–84.

Abidi, N., and M. Manike. 2018. X-ray diffraction and FTIR investigations of cellulose deposition during cotton fiber development. Text. Res. J. 88:719–730.

Abidi, N., E. Hequet, L. Cabrales, J. Gannaway, T. Wilkins, and L.W. Wells. 2008. Evaluating cell wall structure and composition of developing cotton fibers using Fourier transform infrared spectroscopy and thermogravimetric analysis. J. Appl. Polym. Sci. 107:476–486.

Abidi, N., E. Hequet, and L. Cabrales. 2010a. Changes in sugar composition and cellulose content during the secondary cell wall biogenesis in cotton fibers. Cellulose. 17:153–160.

Abidi, N., L. Cabrales, and E. Hequet. 2010b. Fourier transform infrared spectroscopic approach to the study of the secondary cell wall development in cotton fiber. Cellulose. 17:309–320.

Abidi, N., L. Cabrales, and C.H. Haigler. 2014. Changes in the cell wall and cellulose content of developing cotton fibers investigated by FTIR spectroscopy. Carbohyd. Polym. 100:9–16.

Arslan, F.N., G. Akin, S.N.K. Elmas, I. Yilmaz, H-G. Janssen, and A. Kenar. 2019. Rapid detection of authenticity and adulteration of cold pressed black cumin seed oil: A comparative study of ATR–FTIR spectroscopy and synchronous fluorescence with multivariate data analysis. Food Control. 98:323–332.

Bekiaris, G., S. Bruun, C. Peltre, S. Houot, and L.S. Jensen. 2015. FTIR–PAS: A powerful tool for characterising the chemical composition and predicting the labile C fraction of various organic waste products. Waste Manag. 39:45–56.

Bekiaris, G., C. Peltre, S.T. Barsberg, S. Bruun, K.M. Sørensen, S.B. Engelsen, J. Magid, M. Hansen, and L.S. Jensen. 2020. Comparison of three different FTIR sampling techniques (diffuse reflectance, photoacoustic and attenuated total reflectance) for the characterisation of bio-organic samples. J. Environ. Qual. 49:1310–1321. https://doi.org/10.1002/jeq2.20106

Chen, J., X. Chen, Q. Zhu, F. Chen, X. Zhao, and Q. Ao. 2013. Determination of the domain structure of the 7S and 11S globulins from soy proteins by XRD and FTIR. J. Sci. Food Agric. 93:1687–1691.

Chen, N., J. Huang, and K. Li. 2020. Investigation of a formaldehyde-free cottonseed flour-based adhesive for interior plywood. BioResour. 15:5546–5557.

Chen, W., J. Ding, X. Yan, W. Yan, M. He, and G. Yin. 2019. Plasticization of cottonseed protein/polyvinyl alcohol blend films. Polymers. 11:2096.

Cheng, H.N., A. Villalpando, M.W. Easson, and M.K. Dowd. 2017. Characterization of cottonseed protein isolate as a paper additive. Int. J. Polymer Anal. Character. 22:699–708.

Cheng, H.N., K. Kilgore, C. Ford, C. Fortier, M.K. Dowd, and Z. He. 2019. Cottonseed protein-based wood adhesive reinforced with nanocellulose. J. Adhes. Sci. Technol. 33:1357–1368.

Cheng, H.N., Z. He, C. Ford, W. Wyckoff, and Q.Wu. 2020. A review of cottonseed protein chemistry and non-food applications. Sustain. Chem. 1:256–274.

Church, J.S., and A.L. Woodhead. 2017. Cotton fiber wax and surface properties. p. 21–41 *In* S. Gordon and N. Abidi (Eds.), Cotton Fibers: Characteristics, Uses and Performance. Nova Science Publishers, New York, NY.

Dave, H., L. Ledwani, N. Chandwani, N. Chauhan, and S.K. Nema. 2014. The removal of impurities from gray cotton fabric by atmospheric pressure plasma treatment and its characterization using ATR-FTIR spectroscopy. J. Text. Ins. 105(6):586–596.

Durak, T., and J. Depciuch. 2020. Effect of plant sample preparation and measuring methods on ATR-FTIR spectra results. Environ. Exper. Bot. 169:103915.

Egbuta, M., S. McIntosh, D. Waters, T. Vancov, and L. Liu. 2017. Biological importance of cotton by-products relative to chemical constituents of the cotton plant. Molecules. 22:93.

Fang, D. (Ed.). 2018. Cotton Fiber: Physics, Chemistry and Biology. Springer, Cham, Switzerland.

Fang, D.D., and R.G. Percy. 2015. (Eds). Cotton (2nd ed.) Agronomy Monogr. 57. American Society of Agronomy, Inc., Crop Science Society of America, Inc., and Soil Science Society of America, Inc., Madison, WI.

Fortier, C.A., J.E. Rodgers III, and J.A. Foulk. 2015a. Botanical trash mixtures analyzed with near-infrared and attenuated total reflectance fourier transform spectroscopy and thermogravimetric analysis. J. Cotton Sci. 19:603–612.

Fortier, C.A., C.M. Santiago, and J.E. Rodgers III. 2015b. Fourier transform infrared macro-imaging of botanical cotton trash. AATCC J. Res. 2(6):1–6.

Fortier, C.A., C.M. Santiago, J. Rodgers, K. Fontenot, and D. Peralta. 2017. Fourier-transform imaging of cotton and botanical and field trash mixtures. Fibers. 5(20):1–11.

Gaddam, S.K., and A. Palanisamy. 2017. Anionic waterborne polyurethane-imide dispersions from cottonseed oil based ionic polyol. Ind. Crops Prod. 96:132-139.

Gaikwad, M.S., V.V. Gite, P.P. Mahulikar, D.G. Hundiwale, and O.S. Yemul. 2015. Eco-friendly polyurethane coatings from cottonseed and karanja oil. Progress Org. Coat. 86:164–172.

Gordon, S., and N. Abidi. 2017. Cotton Fibers: Characteristics, Uses and Performance. Nova Science Publishers, New York, NY.

Gordon, S., and Y.L. Hsieh. 2007. Cotton: Science and Technology. Woodhead Publishing Limited, Cambridge, England.

Guo, M., Y. Shen, and Z. He. 2012. Poultry litter-based biochar: preparation, characterization, and utilization. p. 71–202 *In* Z. He (Ed.), Applied Research of Animal Manure: Challenges and Opportunities Beyond the Adverse Environmental Concerns. Nova Science Publishers Inc., New York, NY.

He, Z., and H.N. Cheng. 2017. Preparation and utilization of water washed cottonseed meal as wood adhesives. p. 156–178 *In* Z. He (Ed.), Bio-based Wood Adhesives: Preparation, Characterization, and Testing. CRC Press, Boca Raton, FL.

He, Z., C.W. Honeycutt, T. Zhang, and P.M. Bertsch. 2006. Preparation and FT-IR characterization of metal phytate compounds. J. Environ. Qual. 35:1319–1328.

He, Z., C. Du, and J. Zhou. 2011. Structural and bonding environments derived from infrared spectroscopic studies. p. 23–42 *In* Z. He (Ed.), Environmental Chemistry of Animal Manure. Nova Science Publishers Inc., New York, NY.

He, Z., H. Cao, H.N. Cheng, H. Zou, and J.F. Hunt. 2013. Effects of vigorous blending on yield and quality of protein isolates extracted from cottonseed and soy flours. Mod. Appl. Sci. 7(10):79–88. doi:10.5539/mas.v7n10p79

He, Z., D.C. Chapital, H.N. Cheng, and M.K. Dowd. 2014a. Comparison of adhesive properties of water- and phosphate buffer-washed cottonseed meals with cottonseed protein isolate on maple and poplar veneers. Int. J. Adhes. Adhes. 50:102–106.

He, Z., H.N. Cheng, D.C. Chapital, and M.K. Dowd. 2014b. Sequential fractionation of cottonseed meal to improve its wood adhesive properties. J. Am. Oil Chem. Soc. 91:151–158.

He, Z., H. Zhang, and D.C. Olk. 2015. Chemical composition of defatted cottonseed and soy meal products. PLOS One. 10(6):e0129933.

He, Z., S.M. Uchimiya, and M. Guo. 2016. Production and characterization of biochar from agricultural by-products: Overview and use of cotton biomass residues. p. 63–86 *In* M. Guo, Z. He, and S.M. Uchimiya (Eds.) Agricultural and Environmental Applications of Biochar: Advances and Barriers. Soil Science Society of America, Inc., Madison, WI.

He, Z., M. Guo, R.L. Sleighter, H. Zhang, C.A. Fortier, and P.G. Hatcher. 2018a. Characterization of defatted cottonseed meal-derived pyrolysis bio-oil by ultrahigh resolution electrospray ionization Fourier transform ion cyclotron resonance mass spectrometry. J. Anal. Appl. Pyrol. 136:96–106.

He, Z., D. Zhang, and H. Cao. 2018b. Protein profiling of water and alkali soluble cottonseed protein isolates. Sci. Rep. 8:9306.

He, Z., H.N. Cheng, O.M. Olanya, J. Uknalis, X. Zhang, B.D. Koplitz and J. He, 2018c. Surface characterization of cottonseed meal products by SEM, SEM-EDS, XRD and XPS analysis. J. Mater. Sci. Res. 7(1):28–40.

He, Z., D.C. Olk, H. Tewolde, H. Zhang, and M. Shankle. 2020a. Carbohydrate and amino acid profiles of cotton plant biomass products. Agriculture. 10:2.

He, Z., D. Zhang, and O.M. Olanya. 2020b. Antioxidant activities of the water-soluble fractions of glandless and glanded cottonseed protein. Food Chem. 325:126907.

He, Z., H.N. Cheng, and S. Nam. 2021a Comparison of the wood bonding performance of water-and alkali-soluble cottonseed protein fractions. J. Adhes. Sci. Technol. 34: 1500-1517. https://doi.org/10.1080/01694243.2020.1850612

He, Z., M. Guo, C. Fortier, X. Cao, and K. Schmidt-Rohr. 2021b. Fourier transform infrared and solid state ^{13}C nuclear magnetic resonance spectroscopic characterization of defatted cottonseed meal-based biochars. Mod. Appl. Sci. 15 (1):108–121.

He, Z., S. Nam, D.D. Fang, H.N. Cheng, and J. He. 2021c. Surface and thermal characterization of cotton fibers of phenotypes differing in fiber length. Polymers. 13:994.

He, Z., C.P. Mattison, D. Zhang, and C.C. Grimm. 2021d. Vicilin and legumin storage proteins are abundant in water and alkali soluble protein fractions of glandless cottonseed. Sci. Rep. 11:9209.

Hequet, E.F., and N. Abidi. 2006. Sticky Cotton: Measurements and Fiber Processing. Texas Tech Univ Press, Lubbock, TX.

Himmelsbach, D.S., D.E. Akin, J. Kim, and I.R. Hardin. 2003. Chemical structural investigation of the cotton fiber base and associated seed coat: Fourier-transform infrared mapping and histochemistry. Text. Res. J. 73:281–288.

Himmelsbach, D.S., J.W. Hellgeth, and D.D. McAlister. 2006. Development and use of an attenuated total reflectance/ Fourier transform infrared (ATR/FT-IR) spectral database to identify foreign matter in cotton. J. Agric. Food Chem. 54:7405–7412.

Islam, M.S., D.D. Fang, G.N. Thyssen, C.D. Delhom, Y. Liu, and H.J. Kim. 2016. Comparative fiber property and transcriptome analyses reveal key genes potentially related to high fiber strength in cotton (*Gossypium hirsutum* L.) line MD52ne. Biomed. Central (BMC) Plant Biol. 16:36.

Jia, L.K., L.X. Gong, W.J. Li, and C.Y. Kan. 2011. Synthesis of vegetable oil based polyol with cottonseed oil and sorbitol derived from natural source. Chin. Chem. Let. 22:1289–1292.

Kaur, A., B. Singh, A. Kaur, and N. Singh. 2019. Chemical, thermal, rheological and FTIR studies of vegetable oils and their effect on eggless muffin characteristics. J. Food Process. Preser. 43:e13978.

Kim, H.J., Y. Tang, H.S. Moon, C.D. Delhom, and D.D. Fang. 2013a. Functional analyses of cotton (*Gossypium hirsutum* L.) immature fiber (*im*) mutant infer that fiber cell wall development is associated with stress responses. BMC Genomics. 14:889.

Kim, H.J., H.S. Moon, C.D. Delhom, L. Zeng, and D.D. Fang. 2013b. Molecular markers associated with the immature fiber (*im*) gene affecting the degree of fiber cell wall thickening in cotton (*Gossypium hirsutum* L.). Theor. Appl. Genet. 126:23–31.

Kim, H.J., Y. Liu, M.K. Dowd, J.E. Frelichowski, C.D. Delhom. J.E. Rodgers III, and D.P. Thibodeaux. 2016. Comparative phenotypic analysis of *Gossypium raimondii* with Upland cotton. J. Cotton Sci. 20:132–144.

Kim, H.J., Y. Liu, D.D. Fang, and C.D. Delhom. 2019. Feasibility assessment of phenotyping cotton fiber maturity using infrared spectroscopy and algorithms for genotyping analyses. J. Cotton Res. 2:8.

Kirkan, B., C. Sarikurkcu, M. Copuroglu, M. Cengiz, and B. Tepe. 2018. Is it possible to use the stalks of *Gossypium hirsutum* L., an important by-product of cotton cultivation, as an alternative source of bioactive components? Eur. Food Res. Technol. 244:1065–1071.

Kljun, A., H.M. El-Dessouky, T.A. Benians, F. Goubet, F. Meulewaeter, J.P. Knox and R.S. Blackburn. 2014. Analysis of the physical properties of developing cotton fibres. Eur. Polymer J. 51:57–68.

Kramar, A.D., B.M. Obradović, A. Vesel, M.M. Kuraica, and M.M. Kostic. 2018. Surface cleaning of raw cotton fibers with atmospheric pressure air plasma. Cellulose. 25:4199–4209.

Kurtulbaş, E., M. Bilgin, and S. Şahin. 2018. Assessment of lipid oxidation in cottonseed oil treated with phytonutrients: Kinetic and thermodynamic studies. Ind. Crops Prod. 124:593–599.

Kutlu, O., and G. Kocar. 2018. Upgrading lignocellulosic waste to fuel by torrefaction: Characterisation and process optimization by response surface methodology. Int. J. Energy Res. 42:4746–4760.

Lee, C.M., K. Kafle, D.W. Belias, Y.B. Park, R.E. Glick, C.H. Haigler, and S.H. Kim. 2015. Comprehensive analysis of cellulose content, crystallinity, and lateral packing in *Gossypium hirsutum* and *Gossypium barbadense* cotton fibers using sum frequency generation, infrared and Raman spectroscopy, and X-ray diffraction. Cellulose. 22:971–989.

Li, J., S. Pradyawong, Z. He, X.S. Sun, D. Wang, H.N. Cheng, and J. Zhong. 2019. Assessment and application of phosphorus/calcium-cottonseed protein adhesive for plywood production. J. Clean. Prod. 229:454–462.

Li, N., S. Prodyawong, Z. He, X.S. Sun, and D. Wang. 2017. Effect of drying methods on the physicochemical properties and adhesion performance of water-washed cottonseed meal. Ind. Crop. Prod. 109:281–287.

Ling, Z., T. Wang, M. Makarem, C.M. Santiago, H. Cheng, X. Kang, M. Bacher, A. Potthast, and T. Rosenau. et al. 2019. Effects of ball milling on the structure of cotton cellulose. Cellulose. 26:305–328.

Liu, M., Y. Wang, Y. Wu, Z. He, and H. Wan. 2018. "Greener" adhesives composed of urea-formaldehyde resin and cottonseed meal for wood-based composites. J. Clean. Prod. 187:361–371.

Liu, Y. 2015. Rapid and routine assessment of cotton fiber cellulose maturity: current and future trends. p. 17–25 *In* M.I.H. Mondel (Ed.), Cellulose and Cellulose Derivatives: Synthesis, Modification and Applications. Nova Science Publishers, Inc., New York, NY.

Liu, Y., and H.J. Kim. 2015. Use of attenuated total reflection Fourier transform infrared (ATR FT-IR) spectroscopy in direct, non-destructive, and rapid assessment of developmental cotton fibers grown in planta and in culture. Appl. Spectrosc. 69:1004–1010.

Liu, Y., and H.J .Kim. 2017a. Characterization of developmental immature fiber (*im*) mutant and Texas Marker-1 (TM-1) cotton fibers by Attenuated Total Reflection Fourier Transform Infrared (ATR FT-IR) spectroscopy. Appl. Spectrosc. 71(7):1689–1695.

Liu, Y., and H.J. Kim. 2017b. Fourier transform infrared spectroscopy (FT-IR) and simple algorithm analysis for rapid and non-destructive assessment of developmental cotton fibers. Sensors. 17:1469.

Liu, Y., and H.J. Kim. 2019. Comparative investigation of secondary cell wall development in cotton fiber near isogenic lines using attenuated total reflection fourier transform infrared spectroscopy (ATR FT-IR). Appl. Spectrosc. 73(3):329–336.

Liu, Y., and H.J. Kim. 2020. Separation of underdeveloped from developed cotton fibers by attenuated total reflection Fourier transform infrared spectroscopy. Microchem. J. 158:105152.

Liu, Y., D. Thibodeaux, and G. Gamble. 2011. Development of Fourier transform infrared spectroscopy in direct, non-destructive, and rapid determination of cotton fiber maturity. Text. Res. J. 81:1559–1567.

Liu, Y., D. Thibodeaux, G. Gamble., P. Bauer, and D. Van Derveer. 2012. Comparative investigation of Fourier transform infrared (FT-IR) spectroscopy and X-ray diffraction (XRD) in the determination of cotton fiber crystallinity. Appl. Spectrosc. 66:983–986.

Liu, Y., D. Thibodeaux, G. Gamble, and J. Rodgers. 2014. Preliminary study of relating cotton fiber tenacity and elongation with crystallinity. Text. Res. J. 84:1829–1839.

Liu, Y., Z. He, and M. Uchimiya. 2015. Comparison of biochar formation from various agricultural by-products using FTIR spectroscopy. Modern Appl. Sci. 9(4):246–253.

Liu, Y., Z. He, M. Shankle, and H. Tewolde. 2016. Compositional features of cotton plant biomass fractions characterized by attenuated total reflection Fourier transform infrared spectroscopy. Ind. Crop. Prod. 79:283–286.

Liu, Y., H.J. Kim, C.D. Delhom, and D. Thibodeaux. 2019 Investigation of fiber maturity measurement by cross-sectional image analysis and Fourier transform infrared spectroscopy on developing and developed upland cottons. Cellulose. 26:5865–5875.

Liyanage, S., and N. Abidi. 2019. Molecular weight and organization of cellulose at different stages of cotton fiber development. Text. Res. J. 89:726–738.

Ma, M., Y. Ren, W. Xie, D. Zhou, S. Tang, M. Kuang, Y. Wang, and S.K. Du. 2018. Physicochemical and functional properties of protein isolate obtained from cottonseed meal. Food Chem. 240:856–862.

Mahesar, S.A., S.N. Shah, A.W. Mahesar, A.A. Kandhro, A.R. Khaskheli, P. Menghwar, and S.T.H. Sherazi. 2017. A chemometric approach for the quantification of free fatty acids in cottonseed oil by Fourier transform infrared spectroscopy. Inter. J. Food Propert. 20:1913–1920.

Meshram, P.D., R.G. Puri, A.L. Patil, and V.V. Gite. 2013. Synthesis and characterization of modified cottonseed oil based polyesteramide for coating applications. Prog. Organic Coatings.76:1144–1150.

Nam, S., B.D. Condon, Y. Liu, and Q. He. 2017. Natural resistance of raw cotton fiber to heat evidenced by the suppressed depolymerization of cellulose. Polym. Degrad. Stabil. 138:133–141.

Narute, P., and A. Palanisamy. 2016. Study of the performance of polyurethane coatings derived from cottonseed oil polyol. J. Coat. Technol. Res. 13:171–179.

Pereira, A.M.M., M.C. Lopes, J.M.K. Timmer, and J.T.F. Keurentjes. 2005. Solvent sorption measurements in polymeric membranes with ATR-IR spectroscopy. J. Membrane Sci. 260:174–180.

Pradyawong, S., J. Li, Z. He, X.S. Sun, D. Wang, H.N. Cheng, and K.T. Klasson. 2018. Blending cottonseed meal products with different protein contents for cost-effective wood adhesive performances. Ind. Crop. Prod. 126:31–37.

Rathore, K.S., D. Pandeya, L.M. Campbell, T.C. Wedegaertner, L. Puckhaber, R.D. Stipanovic, J.S. Thenell, S. Hague, and K. Hake. 2020. Ultra-low gossypol cottonseed: Selective gene silencing opens up a vast resource of plant-based protein to improve human nutrition. Critic. Revi. Plant Sci. 39:1–29.

Ren, J., N. Li, L. Li, J.K. An, L. Zhao, and N.Q. Ren. 2015. Granulation and ferric oxides loading enable biochar derived from cotton stalk to remove phosphate from water. Bioresour. Technol. 178:119–125.

Santiago, C.M., and D.J. Hinchliffe. 2015. FT-IR examination of the development of secondary cell wall in cotton fibers. Fibers. 3:30–40.

Santiago, C.M., D.J. Hinchliffe, Jr. JG. Montalvo, T.M. Von Hoven, J.E. Rodgers III, G.N. Thyssen, and L. Zeng. 2016. Infrared imaging of cotton fiber bundles using a focal plane array detector and a single reflectance accessory. Fibers. 4:27.

Santiago, C.M., C.A. Fortier, D.J. Hinchliffe, and J.E. Rodgers III. 2017. Chemical imaging of secondary cell wall development in cotton fibers using a mid-infrared focal-plane array detector. Text. Res. J. 87:1040–1051.

Shah, S., S.A. Mahesar, K.A. Abro, S.T.H. Sherazi, and S.M. Nizamani. 2017. FTIR characterization and physico-chemical evaluation of cottonseed oil. Pak. J. Anal. Environ. Chem. 18:46–53.

Silwal, D.K., N. Phambu, B. Pokharel, and A.N. Aziz. 2017. Identification of hydrated and dehydrated lipids and protein secondary structures in seeds of cotton (*Gossypium hirsutum*) line. Pure App. Biol. 6:965–975.

Singh, A., and A. Kaur. 2019. Comparative studies on seed protein characteristics in eight lines of two *Gossypium* species. J. Cotton Res. 2:6.

Song, W., X. Kong, Y. Hua, X. Li, C. Zhang, and Y. Chen. 2020. Antioxidant and antibacterial activity and in vitro digestion stability of cottonseed protein hydrolysates. LWT. 118:108724.

Talpur, M.Y., H. Kara, S.T.H. Sherazi, H.F. Ayyildiz, M. Topkafa, F.N. Arslan, S. Naz, and F. Sirajuddin. 2014. Application of multivariate chemometric techniques for simultaneous determination of five parameters of cottonseed oil by single bounce attenuated total reflectance Fourier transform infrared spectroscopy. Talanta. 129:473–480.

Uchimiya, M., T. Ohno, and Z. He. 2013. Pyrolysis temperature-dependent release of dissolved organic carbon from plant, manure, and biorefinery wastes. J. Anal. Appl. Pyroly. 104:84–94.

Updegraff, D.M. 1969. Semimicro determination of cellulose in biological materials. Anal. Biochem. 32:420–424.

Viles, F.J., and L. Silverman. 1949. Determination of starch and cellulose with anthrone. Anal. Chem. 21:950–953.

Wakelyn, P.J., and M.R. Chaudhry. 2010. (Eds). Cotton: Technology for the 21st Century. International Cotton Advisory Committee, Washington, D.C..

Wakelyn, P.J., N.R. Bertoniere, A.D. French, D.P. Thibodeaux, B.A. Triplett, A.A. Rousselle, Jr. W.R. Goynes, J.V. Edwards, L. Hunter., D.D. Mcalister, and G.R. Gamble. 2007. Cotton Fiber Chemistry and Technology. CRC Press, Boca Raton, FL.

Wang, Q., X. Fan, W. Gao, and J. Chen, 2006. Characterization of bioscoured cotton fabrics using FT-IR ATR spectroscopy and microscopy techniques. Carbohydr. Res. 341:2170–2175.

Yan, H., Z. Hua, G. Qian, M. Wang, G. Du, and J. Chen. 2009. Analysis of the chemical composition of cotton seed coat by fourier-transform infrared (FT-IR) microspectroscopy. Cellulose.16:1099–1107.

Yue, H.-B., Y.-D. Cui, P.S. Shuttleworth, and J.H. Clark. 2012. Preparation and characterization of bioplastics made from cottonseed protein. Green Chem. 14:2009–2016.

Yue, H., Y. Zheng, P. Zheng, J. Guo, J.P. Fernández-Blázquez, J.H. Clark, and Y. Cui. 2020. On the improvement of properties of bioplastic composites derived from wasted cottonseed protein by rational cross-linking and natural fiber reinforcement. Green Chem. 22:8642–8655.

Zhang. B., Y. Cui, G. Yin, X. Li, and Y. You. 2010. Synthesis and swelling properties of hydrolyzed cottonseed protein composite superabsorbent hydrogel. Int. J. Polym. Mater. Polym. Biomater. 59:1018–1032.

Zhang, L., S. Zhang, P. Xu, X. Li, Z. Zhang, S. Fan, J. Gong, Y. Yuan, H. Shang, and H. Zou. 2020. Study crystallinity of the developing cotton fibers by micro-Fourier transform infrared spectroscopy (FTIR) and X-ray diffraction (XRD). Cotton Sci. 32:370–380.

Zhang, L., X. Li, S. Zhang, Q. Gao, Q. Lu, R. Peng, P. Xu, H. Shang, Y. Yuan, and H. Zou. 2021. Micro-FTIR combined with curve fitting method to study cellulose crystallinity of developing cotton fibers. Anal. Bioanal. Chem. 413:1313–1320. https://doi.org/10.1007/s00216-020-03094-6.

Zhao, X., F. Chen, W. Xue, and L. Lee. 2008. FTIR spectra studies on the secondary structures of 7S and 11S globulins from soybean proteins using AOT reverse micellar extraction. Food Hydrocoll. 22:568–575.

Zhou, L., H. He, M. Li.C., K. Song, H. Cheng, and Q.Wu. 2016. Morphological influence of cellulose nanoparticles (CNs) from cottonseed hulls on rheological properties of polyvinyl alcohol/CN suspensions. Carbohyd. Polym. 153:445–454.

Zhou, L., H. He, M.C. Li, S. Huang, C. Mei, and Q. Wu. 2018. Enhancing mechanical properties of poly (lactic acid) through its in-situ crosslinking with maleic anhydride-modified cellulose nanocrystals from cottonseed hulls. Ind. Crop. Prod. 112:449–459.

Zhou, Q., W. Gong, C. Xie, D. Yang, X. Ling, X. Yuan, S. Chen, and X. Liu. 2011. Removal of neutral red from aqueous solution by adsorption on spent cottonseed hull substrate. J. Hazard. Materials. 185:502–506.